Simulation of Transonic Airfoil Flow Using a Zonal RANS-LES Method

Alibek Issakhov[1(✉)], Benedikt Roidl[2], Matthias Meinke[2], and Wolfgang Schröder[2]

[1] Al-Farabi Kazakh National University, Al-Farabi ave. 71, 050040 Almaty, Kazakhstan
alibek.issakhov@gmail.com
[2] Institute of Aerodynamics, RWTH Aachen University, Wüllnerstraße 5a, Aachen, Germany

Abstract. This paper presents a method for a synthetic turbulence generation (STG) to be used in a segregated hybrid Reynolds-averaged Navier-Stokes (RANS)-Large-Eddy Simulation (LES) approach. The present method separates the LES inflow plane into three sections where a local velocity signal is decomposed from the turbulent flow properties of the upstream RANS solution. Depending on the wall-normal position in the boundary layer, the local flow Reynolds and Mach number specific time, length and velocity scales with different vorticity contents are imposed on the LES inflow plane. The STG method is assessed by comparing the resulting skin-friction, velocity and Reynolds-stress distributions of zonal RANS-LES simulations of flat plate boundary layers with available pure LES, DNS, and experimental data. It is shown that for the presented flow cases a satisfying agreement within a short RANS-to-LES transition of two boundary-layer thicknesses is obtained. The method is further used for the simulation of a shock-boundary-layer interaction around an airfoil at transonic flow conditions, where the separated flow region are analyzed by an embedded LES and the remaining flow is determined by a RANS solution.

Keywords: Zonal RANS/LES · Synthetic turbulence · Boundary layer

1 Introduction

CFD simulations at high Reynolds numbers for technical applications are nowadays mainly based on solutions of the Reynolds averaged Navier-Stokes (RANS) equations. The main reason are that they are simple to apply and computationally more efficient than other turbulence modelling approaches such as LES.It is known, however, that in many flow problems the condition of a turbulent equilibrium is not satisfied, i.e., when strong pressure gradients or flow separation occurs, which reduces the prediction accuracy of the results obtained by one- and two-equation turbulence models used to close the RANS equations [13,15].

Alternatives to RANS solutions are direct numerical and large-eddy simulation (DNS and LES). The limits of todays available computer resources, however, still prevent these methods to become standard simulation tools for high

N. Danaev et al. (Eds.): CITech 2015, CCIS 549, pp. 53–65, 2015.
DOI: 10.1007/978-3-319-25058-8_6

Reynolds number flows. In many technical flow problems complex flow regions, which require a higher-order turbulence model, only occur in a small part of the domain. Therefore, the combination of the computational efficiency of the RANS approach with an LES or DNS formulation, promising a higher accuracy, is capable to yield physically more correct results at minimized additional costs compared to pure RANS solutions. An overview of such hybrid RANS-LES approaches is given in [8]. There are at least two widely used techniques to couple RANS with LES. The first approach uses a continuous turbulence model, which switches from RANS to LES to close the system of equations in a unified domain, such as the detached-eddy simulation (DES) proposed by Spalart *et al.* [24]. The transition from RANS to LES is triggered by the local grid size and the wall distance, which means that where the mesh is fine enough to resolve relevant energy containing eddies, the eddy viscosity of the RANS model is reduced to a subgrid scale model. This approach suffers, however, from a so called grey zone, which occurs when the DES model is already switched into LES mode, but the larger scales of the turbulence spectrum are not established in the solution yet. Therefore, it is difficult to switch the DES model from RANS to LES mode e.g. in an attached boundary layer.

The second technique uses two or more predefined separate computational zones that are linked via an overlapping region, where the transition from RANS to LES and vice versa occurs. In the RANS zone a coarse mesh is sufficient for the solution, while in the LES regions a fine mesh is used to allow the required resolution of the turbulent scales up to the inertial range. The interface conditions between the RANS and LES regimes constitute the major challenge of this second technique which will be denoted zonal technique in the following. For the transition from RANS to LES the information of the turbulent flow of the RANS domain must be used to generate a physically correct turbulence spectrum within the overlapping zone of the RANS and LES domains. That is, the mean velocity distribution of the RANS solution and turbulent fluctuations are imposed at the inflow boundary of the embedded LES domain.

There exist several possibilities to generate such turbulent fluctuations at the inflow boundary [19]. Batten *et al.* [3] reformulated on the ideas of Kraichnan [14] and Smirnov *et al.* [21] for wall bounded flows. The velocity signal is generated by a sum of sines and cosines with random phases and amplitudes. The wave numbers are calculated from a three-dimensional spectrum and are scaled by the values of the Reynolds-stress tensor. A special wall treatment was applied to elongate near-wall structures. A transition length to physical turbulence of about ten channel half heights was obtained at low Reynolds number channel flow.

Pamiès *et al.* [19] expanded the method of Jarrin *et al.* [10] by dividing the inflow plane of an incompressible flat plate boundary layer into several zones depending on the wall distance. At each zone turbulent eddy shapes are prescribed in the sense of Marusic [17], i.e., these shapes are representative for typical coherent structures of the turbulent boundary layer. This resulted in a good approximation for the low-order statistics of wall-bounded flows and reduced the

transition length to approximately five boundary-layer thicknesses without using control planes downstream of the LES inflow boundary. Note that the analysis is focused on an incompressible boundary layer at a very limited Reynolds number range at zero-pressure gradient. Furthermore, the averaged inflow conditions such as averaged velocity profile and Reynolds stress tensor were extracted from a fully developed LES solution that was computed *a priori*.

In this study, the ansatz of Pamiès *et al.* [19] is modified and generalized such that incompressible and compressible flows at a wide Reynolds number range can be computed by a robust and efficient zonal RANS-LES method. The averaged inflow conditions are provided by a RANS simulation and the RANS-to-LES transition behavior is analyzed in detail.

The paper is organized as follows. In Section 2, the numerical flow solver and the synthetic turbulence generation method are described. Subsequently, in Section 3 the flow problems, i.e., the flat-plate flows are introduced. Section 4 contains the results. That is, solutions of the zonal method are compared with DNS and experimental findings. Finally, results for the zonal RANS-LES method are presented for a transonic airfoil flow and some concise conclusions are drawn.

2 Numerical Method

2.1 Flow Solver

The three-dimensional unsteady compressible Navier-Stokes equations are solved based on a large-eddy simulation (LES) using the MILES (monotone integrated LES) approach [4]. The vertex-centered finite-volume flow solver is block-structured. A modified advection-upstream-splitting method (AUSM) is used for the Euler terms [16] which are discretized to second-order accuracy by an upwind-biased approximation. For the non-Euler terms a centered approximation of second-order is used. The temporal integration from time level n to $n+1$ is done by a second-order accurate explicit 5-stage Runge-Kutta method, the coefficients of which are optimized for maximum stability. For a detailed description of the flow solver the reader is referred to Meinke *et al.* [18].

The RANS simulations use the one-equation turbulence model of Fares and Schröder [7] to close the averaged equations.

2.2 Synthetic Turbulence Generation Method

The method used in this paper is based on the work of Jarrin *et al.* [10] and Pamiès *et al.* [19], called synthetic eddy method (SEM), which describes turbulence as a superposition of coherent structures. These structures are generated over the LES inlet plane by superimposing the influence of virtual eddy cores that are defined in a specified volume around the inlet plane that has the streamwise, wall-normal, and spanwise dimensions of the turbulent length-scale l_1, the boundary-layer thickness at inlet δ_0, and the width of the computational domain L_z, respectively. N virtual eddy cores are defined at positions x_m^i inside

of the virtual box and their local influence on the velocity field is defined by a shape function σ which describes the spatial and temporal characteristics of the turbulent structure. The normalized stochastical velocity fluctuation components u'_m at the coordinate x_m at the LES inflow plane reads

$$u'_m\left(x_{1,2,3},t\right) = \frac{1}{\sqrt{N}}\sum_{i=1}^{N}\epsilon^i f_{\sigma^m}\left(\tilde{x}_n\right), \tilde{x}_n = \frac{x_n - x_n^i}{l_n}, \tag{1}$$

where the superscript i denotes a virtual eddy core, ϵ^i the random sign, and $m, n = 1, 2, 3$ the Cartesian coordinates in streamwise, wall-normal, and spanwise direction, respectively. . The shape function f_{σ^m} that has a compact support on $[-l_n, l_n]$ where l_n is a length scale which satisfies the normalization condition $\frac{1}{\sqrt{2\pi}}\int_{-1}^{1} f_{\sigma^m}^2\, d\tilde{x}_m = 1$. Jarrin *et al.* used as shape function $f_{\sigma^{m=1,2,3}}$ a Gauss- or a tent function. The virtual eddy cores convect with the velocity U_{con} in streamwise direction. Once $x_1^i > l_1$ a new eddy core assigned with randomly chosen coordinates x_m^i and signs ϵ^i is generated.

The velocity signal at the LES inflow plane is composed of an averaged velocity component which is in this work provided from the upstream RANS solution and the normalized stochastic fluctuation u'_m of Eq. 1 that is subjected to a Cholesky decomposition A_{mn} to assign the values of the Reynolds-stress tensor R_{mn}.

$$u_m\left(x,t\right) = U_{RANS}^m + \sum_n A_{mn} u'_m\left(x,t\right). \tag{2}$$

Pamiès *et al.* [19] extended the method by dividing the inflow plane in several domains p depending on the distance from the wall. Each domain is characterized by specific shape factors, turbulent length- and time scales. Thus, the velocity fluctuation component of Eq. 1 yields

$$u'_m\left(x_{1,2,3},t\right) = \sum_{p=1}^{P} u'_{m,p}\left(x_{1,2,3},t\right) \tag{3}$$

where P denotes the number of divided domains of the inflow plane. Pamiès *et al.* defined the shape function $f_{\sigma_p^n}$ of the first two planes according to the educed turbulent structures of Jeong *et al.* [12],

$$\begin{aligned} f_{\sigma_{p=1,2}^{m=1}} &= G\left(\tilde{x}_1\right) G\left(\tilde{x}_2\right) H\left(\tilde{x}_3\right) \\ f_{\sigma_{p=1,2}^{m=2}} &= -G\left(\tilde{x}_1\right) G\left(\tilde{x}_2\right) H\left(\tilde{x}_3\right) \\ f_{\sigma_{p=1,2}^{m=3}} &= G\left(\tilde{x}_1\right) H\left(\tilde{x}_2\right) G\left(\tilde{x}_3\right) \end{aligned}$$

where $H\left(\tilde{x}_m\right) = 1 - \cos\left(2\pi\tilde{x}_m\right) / \left(2\pi \cdot 0.44\right)$ and $G\left(\tilde{x}_m\right)$ is a Gaussian function.

In this work the inflow plane was divided in three planes, that is $P = 3$. The position in wall-normal direction $x_{2,beg}, x_{2,end}$ of each plane p and the corresponding length scales in streamwise, wall-normal, and spanwise direction, and convection velocities are given in Tab. 1. The length scales of the turbulent structures l_n in the first plane $p = 1$ are chosen accordingly to Pamiès *et al.* [19] and

del Alamo *et al.* [2]. However, the length scales of the structures in the second and third plane $p = 2, 3$ are set to values that are different compared to Pamiès *et al.* The analysis of several incompressible and compressible boundary layers at various Reynolds numbers has shown that the values chosen by Pamiès *et al.* at $p = 2, 3$ did not satisfactorily match the reference flow field.

The shear-stress component $\langle u_1' u_2' \rangle$ of the Reynolds-stress tensor R_{mn} that is needed for Eq.2 is obtained from the RANS solution located upstream of the LES inlet [20]. The normal-stress components are reconstructed using a fourth order polynomial function to match the distribution of Spalart [1].

Morkovin' s hypothesis is applied at the inlet to relate density and velocity fluctuations and to enforce the strong Reynolds analogy (SRA) [22]. The density field is obtained by enforcing a constant-pressure condition at the inflow [6].

Table 1. Locations of planes p, turbulent length scales l_n, and convection velocities U_{con}

plane	$l_{y,p}$ $[x_{2,beg}; x_{2,end}]$	$= l_1$	l_2	l_3	U_{con}
$p = 1$	$[0; (60)^+]$	$(100)^+$	$(20)^+$	$(60)^+$	$0.6U_\infty$
$p = 2$	$[(60)^+; 0.65\delta_0]$	$0.5\delta_0$	$0.3\delta_0$	$0.25\delta_0$	$0.75U_\infty$
$p = 3$	$[0.65\delta_0; 1.2\delta_0]$	$0.3\delta_0$	$0.3\delta_0$	$0.3\delta_0$	$0.9U_\infty$

3 Computational Setup

Flat Plate Boundary Layer. A subsonic flat-plate boundary-layer flow is investigated to validate the STG method for the zonal RANS-LES configuration comparing the results with a pure RANS, pure LES, and available experimental data. The freestream Mach numbers are $M = 0.4$ and $M = 2.3$ and the freestream Reynolds numbers based on the momentum thickness at $x/\delta_0 = 0$ are $Re_\theta = 1400$ and $Re_\theta = 4200$, respectively. where δ_0 denotes the boundary-layer thickness at the inlet of computational domain of the pure LES, pure RANS, and the embedded LES part of the zonal RANS-LES simulation. The inflow boundaries of the pure LES, pure RANS, and the embedded LES part of the zonal RANS-LES simulation are located at $x/\delta_0 = 0$.

The numerical details of each simulation are presented in Tab. 2. The grids are clustered to the surface in the wall-normal direction using a hyperbolic tangent stretching function such that the minimum grid spacing in wall units is approximately one and a stretching factor of 1.05 is not exceeded. Depending on the configuration subsonic and supersonic outflow boundary conditions are used at the upper and downstream boundaries. The no-slip boundary condition is imposed at the adiabatic wall. The inflow distribution of the flow variables for the LES inlet of the zonal RANS-LES simulation were extracted from the RANS part that is located upstream of the LES domain.

Table 2. Computational domain, grid resolution, and number of mesh points for pure LES, pure RANS, and zonal RANS-LES configurations of turbulent boundary layer simulations. The zonal RANS-LES configuration consists of the RANS domains upstream (Zo-RANS) and of the embedded LES domain (Zo-LES).

domain	domain size			resolution			number of grid points		
	L_x/δ_0	L_y/δ_0	L_z/δ_0	Δx^+	Δy^+_{wall}	Δz^+	$i_{\max}$	$j_{\max}$	$k_{\max}$
pure LES ($M = 0.4$)	16.0	3.4	0.88	15.1	1.1	6.7	516	67	49
pure 2D-RANS ($M = 0.4$)	16.0	3.4	-	62.2	1.1	-	104	67	-
Zo-RANS ($M = 0.4$)	4.0	3.4	0.88	61.1	1.1	160	31	67	3
Zo-LES ($M = 0.4$)	12.0	5.0	0.88	15.1	1.1	6.7	387	67	49

The inflow distributions of the pure LES results is determined using the rescaling method of El-Askary *et al.* [6]. The recycling station is located at $x/\delta_0 = 6$. A sponge layer is applied at the upper- and outflow boundary to damp spurious pressure fluctuations. The wall- and velocity outflow boundary conditions are the same as for the formulations of the pure 2D-RANS configuration.

Transonic Airfoil Flow. The transonic flow around a DRA2303 airfoil [9] was chosen as the aerodynamic reference case to discuss the efficiency and quality of the zonal RANS-LES method compared to a pure LES method. The flow field is defined by $M = 0.72$, $Re_c = 2.6 \cdot 10^6$ based on the chord length c, and the angle of attack $\alpha = 3°$. The laminar-turbulent transition is fixed at the pressure and suction side of the airfoil at $x/c = 0.05$ for both numerical configurations by introducing a wall surface roughness of an amplitude of approximately 10 inner wall units or $8 \cdot 10^{-4} \Delta y/c$.

Table 3. Computational domain, grid resolution, and number of mesh points for pure LES and zonal RANS-LES configuration for the transonic airfoil case. The zonal RANS-LES configuration consists of the RANS domains (Zo-RANS) and of the embedded LES domain (Zo-LES).

domain	domain size		resolution			number of grid points			
	L_{farfield}	L_{spanwise}	Δx^+	Δy^+_{wall}	Δz^+	$I_{\max}$	$j_{\max}$	$k_{\max}$	total
pure LES	$25c$	$0.021c$	100	1.0	20	2364	130	97	$30 \cdot 10^6$
Zo-RANS	$25c$	$0.021c$	400	1.0	180	225	89	11	$2.2 \cdot 10^5$
Zo-LES	$0.4c$	$0.021c$	100	1.0	20	1430	97	97	$13.5 \cdot 10^6$

The resolution of the pure LES grid in the streamwise, wall normal and spanwise direction of $\Delta x^+ \approx 100$, $\Delta y^+_{min} \approx 1$, and $\Delta z^+ \approx 20$, respectively, yields a total number of grid points of approximately $30 \cdot 10^6$. The spanwise extension of the grid is 0.021 c. Using the same grid resolution and spanwise extension,

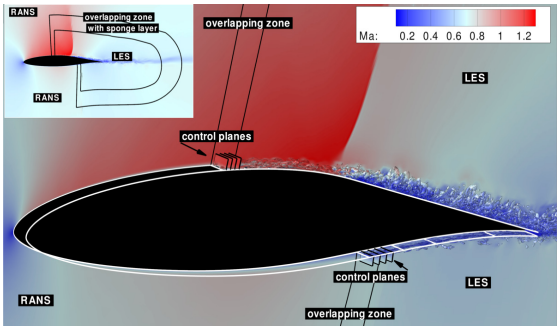

Fig. 1. Computational configuration of the zonal RANS-LES computation and Mach number contours. In the LES zone λ_2-contours [11] are shown color coded with mapped-on local Mach number.

the number of grid points of the embedded LES domain of the zonal RANS-LES configuration is approximately $13.7 \cdot 10^6$, i.e., the reduction is more than a factor of two. Details of the grid configurations are given in Tab. 3. The pure LES uses periodic boundary conditions in the spanwise direction and a no-slip, adiabatic condition is imposed on the wall. Non-reflective boundary conditions are applied to the far field boundaries. The computational setup of the zonal RANS-LES computation is shown in Fig. 1. The zonal RANS-LES configuration uses the same boundary conditions at the wall and in the far field as the pure LES computation. At the inflow boundary of the LES domain on the upper and lower side of the airfoil, the STGM discussed in Sec. 2 is applied to generate synthetic turbulent structures in the turbulent boundary layer. Downstream of the LES inflow boundary at the upper side four control planes are located between $0.37 \leq x/c \leq 0.4$ and at the lower side between $0.7 \leq x/c \leq 0.73$. The time-averaged velocity profile and the Reynolds shear stress component $\langle u'v' \rangle$ of the upstream RANS solution are used as target conditions for the STGM and the control planes. At the RANS outflow the time-averaged pressure from the embedded LES domain located downstream is prescribed whereas density and velocity distributions are extrapolated. At the LES inflow the density and velocity distributions from the upstream RANS domain are imposed and the pressure values are extrapolated from the interior of the embedded LES domain. The LES domain is encompassed by a sponge layer to damp spurious pressure fluctuations.

4 Results

Subsonic Boundary Layer. In this section, the findings of the subsonic flat-plate boundary layer flow applying the STG method for the zonal RANS-LES ansatz are discussed. In the subsequent paragraphs the term zonal RANS-LES is applied for the results of the corresponding embedded LES domain. In Sec. 4 the inflow method is validated for a subsonic flat-plate boundary-layer flow,

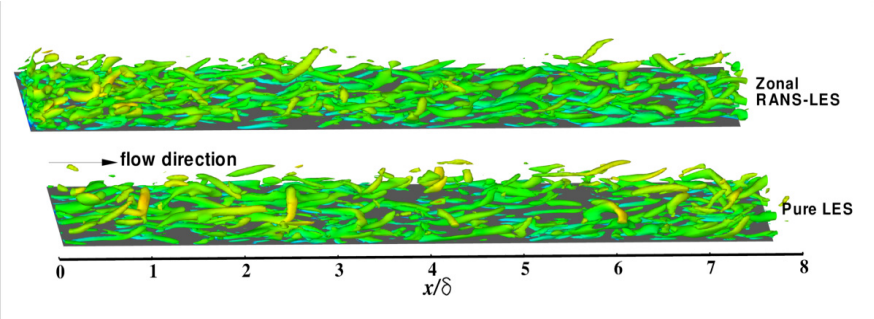

Fig. 2. Coherent turbulent structures based on the λ_2-criterion with mapped-on local Mach number for subsonic flat-plate boundary layer.

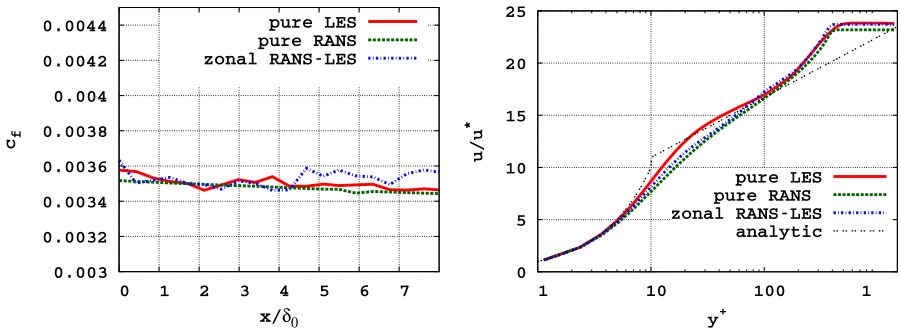

Fig. 3. Skin-friction distributions (left) and van-Driest-velocity distributions at $x/\delta_0 = 2$(right) for several numerical configurations.

respectively, by comparing the averaged boundary-layer properties and turbulent flow field with reference LES, and experimental data. The development of the coherent turbulent structures in the pure LES and zonal RANS-LES solution is discussed and the streamwise distributions of the skin-friction coefficient c_f, the shape factor H, and the displacement thickness δ_1 of the pure LES, and the zonal RANS-LES solution are compared. For the subsonic case the Reynolds shear stress distributions at $x/\delta_0 \approx 2$ of the zonal RANS-LES are compared with pure LES and measurements of deGraaff and Eaton [5].

Coherent turbulent structures based on the λ_2-criterion according to Jeong and Hussain [11] with mapped-on Mach number contours are visualized in Fig. 4 for the zonal RANS-LES solution and the pure LES. Near the inflow boundary of the LES domain of the zonal RANS-LES simulation at $x/\delta_0 < 1$ elongated structures are already visible. At $x/\delta_0 > 1$ the size and number of those structures is comparable to that of the pure LES result. The STG method presented in Sec. 2.2 generates coherent turbulent structures that contain the appropriate length- and time scales which form flow patterns downstream of the inlet that

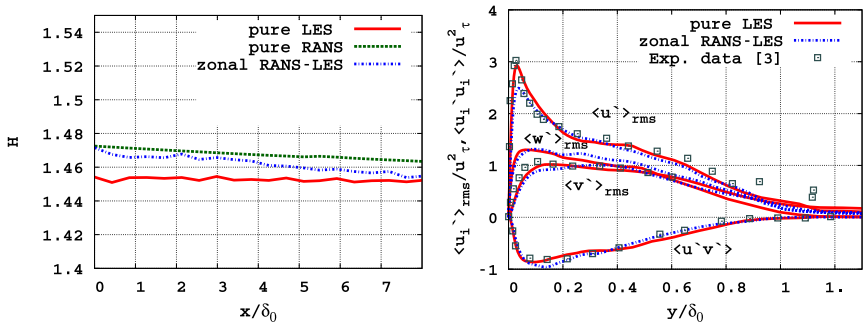

Fig. 4. Streamwise development of the shape-factor (left) for several numerical configurations and comparison of Reynolds normal-stress component distributions of pure LES, zonal RANS-LES, and reference experimental results [5] at $x/\delta_0 = 2$ (right).

resemble the turbulent structures of the pure LES solution. That is, already at $x/\delta_0 \approx 1$ ejected vortices are observed and elongated structures in the streamwise direction that are essential for the turbulence production develop further downstream.

The streamwise development of the skin-friction coefficient c_f is presented in Fig. 3(a). The c_f-distribution for the pure RANS and the zonal RANS-LES results are in good agreement with the pure LES solution. Downstream of the LES inflow of the zonal RANS-LES the skin-friction coefficient does not drop but rather immediately converges to the pure LES values. The structures generated by the original inflow method of Jarrin *et al.* [10] would too strongly dissipate such that a much larger streamwise extent would be necessary for the LES to recover the correct c_f-level.

In Fig. 3(b) the van-Driest velocity distribution at x/δ_0 of pure LES, pure RANS and the zonal RANS-LES simulation is shown. The distribution of the zonal RANS-LES resembles that of the pure RANS, however, it started to converge to the distribution of the pure LES.

Figure 4(a) shows the time-averaged streamwise distribution of the shape factor H. The growth rates of the pure RANS, the pure LES, and the zonal RANS-LES simulation are more or less alike. From the streamwise distributions of the skin-friction coefficient and the displacement thickness it can be concluded that the zonal RANS-LES method yields smooth streamwise results which are comparable with the pure LES findings.

The distributions of the Reynolds normal- and shear-stress components of the pure LES and the zonal RANS-LES configuration are compared with the experimental results $Re_\theta = 1430$ of deGraaff and Eaton [5] in Fig. 4(b). A good agreement with the experimental data is obtained corroborating that the inflow generation method for the zonal RANS-LES configuration is capable of generating physically meaningful Reynolds stresses within a short transition length, i.e., in less than two boundary-layer thicknesses δ_0.

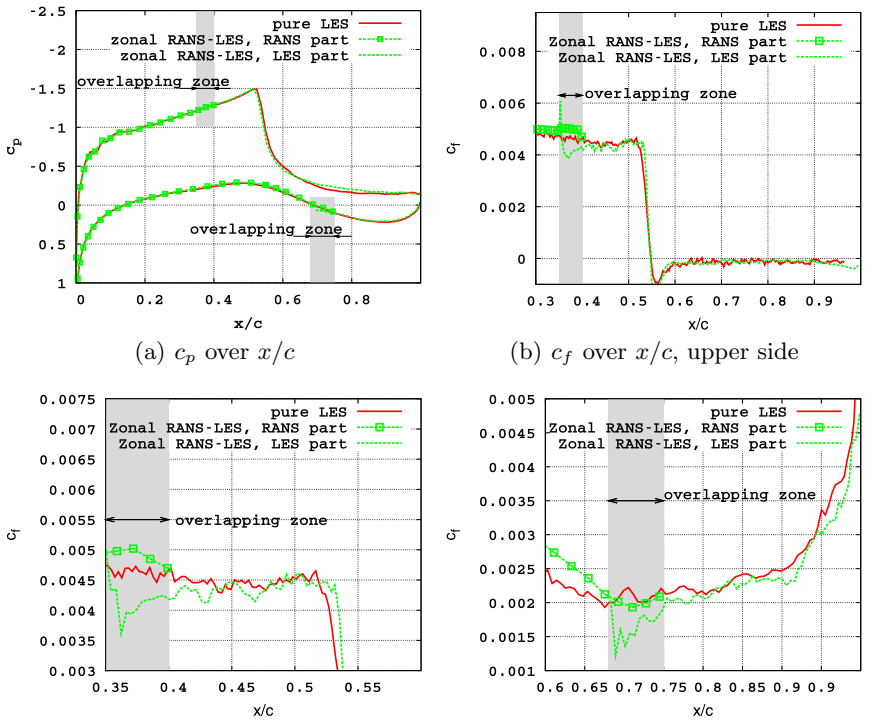

(a) c_p over x/c

(b) c_f over x/c, upper side

(c) c_f over x/c, upper side, close-up

(d) c_f over x/c, lower side

Fig. 5. Pressure coefficient distribution c_p and skin-friction coefficient distribution c_f at the upper and lower side of the DRA2303 airfoil for the zonal RANS-LES and the pure LES.

Transonic Airfoil Flow. In Fig. 5(a) the time- and spanwise averaged distributions of the pressure coefficient c_p for the zonal RANS-LES and the pure LES are presented. The averaging time was about two shock-oscillation cycles. The gray shaded areas represent the overlapping regions of the zonal RANS-LES approach. The average shock position is located at $x/c \approx 0.57$ for the zonal RANS-LES and the pure LES result. A smooth RANS-to-LES transition of the pressure coefficient at the upper and lower side of the airfoil is evident.

The skin-friction coefficient distributions at the upper side of the airfoil are presented in Fig. 5(a). The c_f distribution of the zonal RANS-LES agrees well over the entire upper side of the airfoil with the pure LES result. From the shock position at $x/c \approx 0.57$ to the trailing edge the averaged flow field is fully separated.

In Fig. 6(a) the velocity distribution of the zonal RANS-LES and the pure LES solutions are compared at $x/c = 0.50$ which is located upstream of the average shock position at $x/c \approx 0.57$. A slight deviation near the boundary-layer edge in

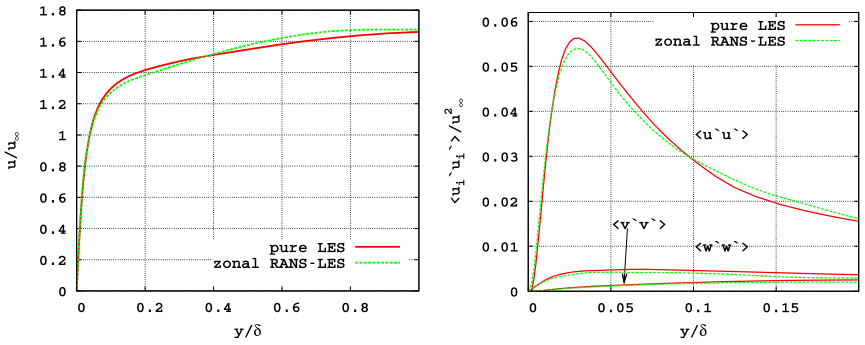

(a) Velocity profile u/u_∞ (b) Reynolds stresses $\langle u_i u_i \rangle / u_\infty^2$

Fig. 6. Velocity profile and normal components of the Reynolds-stress tensor at $x/c = 0.50$ at the upper side of the DRA2303 airfoil for the zonal RANS-LES and the pure LES.

the velocity distribution is observed. However, near the wall the difference between the velocity profiles is small resulting in almost identical c_f-values.

The distributions of the normal components of the Reynolds stress tensor at $x/c = 0.50$ for the zonal RANS-LES and the pure LES computations are shown in Fig. 6(b). The normal stresses computed by the zonal RANS-LES method are in very good agreement with the pure LES results. This convincing match of the velocity and the Reynolds-normal-stress distributions constitute a crucial requirement to obtain similar shock dynamics as well as time-averaged shock positions.

5 Conclusion

A synthetic turbulence generation method for a zonal RANS-LES method for sub- and supersonic flows has been introduced. The STG method has been validated by computing a subsonic boundary-layer flow at $M = 0.4$ and $Re_\theta = 1400$ and a supersonic flow boundary-layer flow at $M = 2.3$ and $Re_\theta = 4200$, respectively. The zonal RANS-LES solutions were compared with pure LES, pure RANS, DNS, and experimental data. A rapid RANS-to-LES transition was observed and the overall accuracy has been convincing. Within a transition length from the RANS to the LES solution of approximately two boundary-layer thicknesses the zonal ansatz showed good agreement in the streamwise c_f distribution, the velocity profiles, and the distribution of the Reynolds stresses compared with measurements [5]. Also the growth rate of boundary-layer-shape factor, the boundary-layer-displacement thickness in the streamwise direction of the zonal RANS-LES solution was in good agreement with that of the pure LES results.

The convincing agreement of the zonal RANS-LES results with the pure LES solutions for the transonic airfoil flow increases the confidence in the appli-

cation of the zonal RANS-LES method. Since no modifications of the interface formulations are necessary it is more or less straightforward to apply the zonal RANS-LES method to other three-dimensional sub- and transonic flow problems.

References

1. Spalart, P.R.: Direct simulation of a turbulent boundary layer up to $Re_\theta = 1410$. J. Fluid Mech. **187**, 61–98 (1988)
2. del Alamo, J.C., Jimenez, J., Zandonade, P., Moser, R.D.: Self-similar vortex clusters in the turbulent logarithmic region. J. Fluid Mech. **561**, 329 (2006)
3. Batten, P., Goldberg, U., Chakravarthy, S.: Interfacing statistical turbulence closures with large-eddy simulation. AIAA J. **42**(3), 485–492 (2004)
4. Boris, J.P., Grinstein, F.F., Oran, E.S., Kolbe, R.L.: New insights into large eddy simulation. Fluid Dynamics Research **10**, 199–228 (1992)
5. DeGraaff, D.B., Eaton, J.K.: Reynolds-number scaling of the flat-plate turbulent boundary layer. J. Fluid Mech. **422**, 319–346 (2000)
6. El-Askary, W., Schröoder, W., Meinke, M.: LES of compressible wall-bounded flows. In: AIAA Paper (2003–3554) (2003)
7. Fares, E., Schröoder, W.: A general one-equation turbulence model for free shear and wallbounded flows. Flow, Turbulence and Combustion **73**, 187–215 (2004)
8. von Fröhlich, J., Terzi, D.: Hybrid LES/RANS methods for the simulation of turbulent flows. Prog. Aerospace Sci. **44**, 349–377 (2008)
9. Fulker, J.L., Simmons, M.J.: An Experimental Investigation of Passive Shock/Boundary Layer Interaction Control on an Aerofoil. Draiasihwaicr 9521611 EUROSHOCK Tr Aer 2 4913(2) (1992)
10. Jarrin, N., Benhamadouche, S., Laurence, D., Prosser, R.: A synthetic-eddy-method for generating inflow conditions for large-eddy simulations. Int. J. Heat Fluid Flow **27**, 585–593 (2006)
11. Jeong, J., Hussain, F.: On the identification of a vortex. J. Fluid Mech. **285**, 69–94 (1995)
12. Jeong, J., Hussain, F., Schoppa, W., Kim, J.: Coherent structures near the wall in a turbulent channel flow. J. Fluid Mech. **332**, 185 (1997)
13. Knight, D.D., Yan, H., Panaras, A.G., Zheltovodov, A.A.: Advances in CFD prediction of shock wave turbulent boundary layer interactions. Progress in Aerospace Science **39**, 121–184 (2003)
14. Kraichnan, R.H.: Inertial Ranges in Two-Dimensional Turbulence. Phys. Fluids **10**(7), 1417–1423 (1967)
15. Leschziner, M., Drikakis, D.: Turbulence modelling and turbulent-flow computation in aeronautics. Aeronautical Journal **106**(1061), 349–383 (2002)
16. Liou, M.S., Steffen, C.J.: A new flux splitting scheme. Journal of Computational Physics **107**, 23–39 (1993)
17. Marusic, I.: On the role of large-scale structures in wall turbulence. Physics of Fluids **13**, 735 (2001)
18. Meinke, M., Schröder, W., Krause, E., Rister, T.: A comparison of second- and sixth-order methods for large-eddy simulations. Computers and Fluids **31**, 695–718 (2002)
19. Pamiès, M., Weiss, P.E., Garnier, E., Deck, S., Sagaut, P.: Generation of synthetic turbulent inflow data for large eddy simulation of spatially evolving wall-bounded flows. Physics of Fluids **16**, 045103 (2009)

20. Roidl, B., Meinke, M., Schröder, W.: Zonal RANS/LES computation of transonic airfoil flow. In: AIAA Paper (2011–1056) (2011)
21. Smirnov, A., Shi, S., Celik, I.: Random flow generation technique for large eddy simulations and particle dynamics modeling. J. Fluids Eng. **123**, 359–371 (2001)
22. Smits, A.J., Dussauge, J.P.: Turbulent Shear Layers in Supersonic Flow, 2nd edn. Springer, New York (2006)
23. Spalart, P.: Direct simulation of a turbulent boundary layer up to req = 1410. J. Fluid Mech. **187**, 61–98 (1988)
24. Spalart, P.R., Jou, W.H., Strelets, M., Allmaras, S.R.: Comments on the feasibility of LES for wings, and on a hybrid RANS/LES approach. In: Advances on DNS/LES, pp. 137–147. Greyden Press, Columbus, OH (1997)